1-1-2013

Synthesis of hollow GeO2 nanostructures, transformation into GeOC, and lithium storage properties

Li Li
University of Wollongong, li@uow.edu.au

Kuok H. Seng
University of Wollongong, kseng@uow.edu.au

Chuanqi Feng
Hubei University, China, cfeng@uow.edu.au

Hua-Kun Liu
University of Wollongong, hua@uow.edu.au

Zaiping Guo
University of Wollongong, zguo@uow.edu.au

Synthesis of hollow GeO2 nanostructures, transformation into GeOC, and lithium storage properties

Abstract

In this work, we synthesize mesoporous and hollow germanium@carbon nanostructures through simultaneous carbon coating and reduction of a hollow ellipsoidal GeO2 precursor. The formation mechanism of GeO 2 ellipsoids and the ratio of Ge4+ to Sn4+ as the starting materials are also investigated. Compared to the solid ellipsoidal Ge@carbon (Ge@C-3), the hollow ellipsoidal Ge@C-1 sample exhibits better cycling stability (100% capacity retention after 200 cycles at the 0.2 C rate) and higher rate capability (805 mA h g-1 at 20 C) compared to Ge@C-3 due to its unique hollow structure; therefore, this hollow ellipsoidal Ge@carbon can be considered as a potential anode material for lithium ion batteries. 2013 The Royal Society of Chemistry.

Keywords

storage, properties, c, ge, lithium, into, synthesis, transformation, nanostructures, geo2, hollow

Disciplines

Engineering | Physical Sciences and Mathematics

Publication Details

Li, L., Seng, K. H., Feng, C., Liu, H. K. & Guo, Z. (2013). Synthesis of hollow GeO2 nanostructures, transformation into Ge@C, and lithium storage properties. Journal of Materials Chemistry A, 1 (26), 7666-7672.

Journal of Materials Chemistry A

RSC Publishing

PAPER

View Article Online
View Journal | View Issue

Cite this: J. Mater. Chem. A, 2013, 1, 7666

Synthesis of hollow GeO_2 nanostructures, transformation into Ge@C, and lithium storage properties†

Li Li,[a] Kuok Hau Seng,[ab] Chuanqi Feng,[bc] Hua Kun Liu[a] and Zaiping Guo*[abc]

Received 5th April 2013
Accepted 29th April 2013

DOI: 10.1039/c3ta11381g

www.rsc.org/MaterialsA

In this work, we synthesize mesoporous and hollow germanium@carbon nanostructures through simultaneous carbon coating and reduction of a hollow ellipsoidal GeO_2 precursor. The formation mechanism of GeO_2 ellipsoids and the ratio of Ge^{4+} to Sn^{4+} as the starting materials are also investigated. Compared to the solid ellipsoidal Ge@carbon (Ge@C-3), the hollow ellipsoidal Ge@C-1 sample exhibits better cycling stability (100% capacity retention after 200 cycles at the 0.2 C rate) and higher rate capability (805 mA h g^{-1} at 20 C) compared to Ge@C-3 due to its unique hollow structure; therefore, this hollow ellipsoidal Ge@carbon can be considered as a potential anode material for lithium ion batteries.

Introduction

Rechargeable lithium ion batteries (LIBs) are currently one of the most important energy storage devices for portable electronics. In order to meet the requirements of highly demanding applications, such as electric vehicles, lithium ion batteries with higher power or energy density are needed.[1] This can be achieved by utilizing electrode materials with higher specific capacity than the current commercial electrode materials.[2] In terms of capacity, group IVA elements are the most promising as an anode material for LIBs, particularly silicon and germanium, which have theoretical capacities of 4200 and 1600 mA h g^{-1}, respectively.[1a] Compared to Si-based materials, Ge has attracted less attention due to its higher cost; however, with the increasing interest in Ge as a potential anode material, the cost could gradually decrease. In addition to the high theoretical capacity, the lithium diffusivity and the electrical conductivity of Ge are 400 and 10^4 times higher, respectively, than for Si at room temperature.[3] Furthermore, Ge exhibits a lower specific volume change during the Li insertion/extraction process than Si, which can be expected to lead to better cycling performance at comparable capacity.[3a,b] It has been reported that the mechanical stress, which is related to volume changes in excess of 200%, can induce pulverization and aggregation, as well as loss of the electrical interphase contact, which leads to increased diffusion lengths and poor cycling stability. Therefore, it is crucial to find a solution to reduce the degree of volume change. Several strategies have been proposed to improve the cycling stability of germanium, for example, decreasing the particle size,[4] using elemental alloys,[5] designing unique morphologies,[6] dispersing germanium into an inactive matrix,[7] or using novel electrolytes,[4] but the cycling performance still needs to be further enhanced to meet the increasing demands of next generation LIBs.

Materials with hollow nanostructures have recently attracted considerable interest as an important family of functional materials with technological significance in energy storage and conversion, catalysis, gas sensing, and biomedicine.[8] In terms of lithium ion batteries, the void space in the hollow nanostructure can efficiently increase the active area, accommodate large strain from the alloying reaction of the active material with lithium, and prevent detachment of the active materials from the electrode framework.

Herein, we report on the synthesis of a GeO_2 hollow nanostructure using a one-pot ultrasonication method. In addition, we have investigated the formation mechanism of the

[a]Institute for Superconducting and Electronic Materials, University of Wollongong, North Wollongong, NSW 2500, Australia. E-mail: zguo@uow.edu.au

[b]School of Mechanical, Materials and Mechatronics Engineering, University of Wollongong, Wollongong, NSW 2522, Australia

[c]College of Chemistry & Chemical Engineering, Hubei University, Wuhan 430062, P. R. China

† Electronic supplementary information (ESI) available: Fig. S1: FE-SEM images of GeO_2 precursors synthesized at different reaction times; Fig. S2: X-ray diffraction patterns of GeO_2 precursors at different reaction times; Fig. S3: EDS spectra of GeO_2 precursors at different reaction times with the corresponding FE-SEM images; Fig. S4: X-ray diffraction patterns of Ge@C ellipsoids; Fig. S5: Raman spectra of GeO_2 precursors and Ge@C; Fig. S6: FTIR spectra of GeO_2 precursors and Ge@C; Fig. S7: TGA curves of Ge@C and pure Ge; Fig. S8: nitrogen adsorption–desorption isotherms and Barrett–Joyner–Halenda (BJH) pore size distribution plots (inset) of hollow Ge@C ellipsoids; Fig. S9: FE-SEM images of Ge@C samples at different resolutions; Fig. S10: FE-SEM image of pure Ge after reduction in H_2/Ar; Fig. S11: cyclic voltammograms for the Ge@C-1 sample; Fig. S12: voltage profiles of (a) Ge@C-1 and (b) Ge@C-3 at different rates, (c) cycling performance of Ge@C-1 and Ge@C-3 at the 0.1 C/0.1 C charging–discharging rate for the first 5 cycles, then at the 5 C/0.5 C charging–discharging rate for the rest of the cycling; Fig. S13: rate performance of Ge@C-4 at increasing rates from 1 to 25 C, with the discharging rate fixed at 0.5 C. See DOI: 10.1039/c3ta11381g

ellipsoidal GeO_2 and the effects of $SnCl_4$ on the formation of the hollow structure. As elemental germanium performs better as an anode material for LIBs compared to GeO_2, we have employed a simultaneous carbon coating and thermal reduction method in order to reduce GeO_2 to Ge while maintaining the nanostructure. The germanium@carbon (Ge@C) shows high capacity and excellent cycling stability as an anode material for the LIB.

Experimental section

Hollow ellipsoidal GeO_2 structures were synthesized by hydrolysis of $GeCl_4$ under ultrasonication. In a typical procedure, the molar ratio of Ge to Sn is 1 : 1. 1.635 g of $SnCl_4 \cdot 5H_2O$ was dissolved in 35 mL of ethanol (99.9%, anhydrous, Sigma Aldrich) and left under ultrasonication for 10 min. $GeCl_4$ (99.99%, Alfa, Aesar)/ethanol (1 g/10 mL) solution was then added into the above $SnCl_4$ solution. Subsequently, 7 mL of deionised water and 1 mL of concentrated $NH_3 \cdot H_2O$ were added into the above solution, followed by ultrasonication for 120 min. The white precipitate was collected by centrifugation and rinsed several times with ethanol before drying at 80 °C under vacuum to obtain the GeO_2 hollow ellipsoidal precursor. The precursor was then ready for further processing and characterization. To investigate the formation mechanism of hollow ellipsoidal GeO_2, a series of time-dependent experiments (5, 30, 50, 90 min under ultrasonication) was also conducted. Furthermore, in order to clarify the effects of $SnCl_4$ on the morphology, two ratios of Ge to Sn (1 : 0.5, 1 : 0) were also used to make samples under the same conditions. The precursors with ratios of 1 : 1, 1 : 0.5, and 1 : 0 were denoted as GeO_2-1, GeO_2-2, and GeO_2-3, respectively.

Hollow carbon ellipsoids containing germanium nanoparticles (denoted as "Ge@C") were synthesized by the chemical vapour deposition (CVD) method in a horizontal tube furnace. The gases used in the experiment were 5% H_2 in argon, 10% C_2H_2 in argon, and 99.99% argon. In a typical procedure, the GeO_2 precursor was firstly heated to 650 °C in the flowing C_2H_2/Ar mixture and kept at that temperature for 30 min. The C_2H_2/Ar mixture was then replaced by a H_2/Ar mixture, and the flow continued for 2 h. The furnace was then left to cool to room temperature in an Ar atmosphere. The heating rate used throughout the experiment was 5 °C min^{-1}. For comparison, the pure Ge sample was annealed under the same conditions, but without the flowing C_2H_2.

Materials characterization

The structure and morphology of the as-prepared samples were characterized by X-ray diffraction (XRD; MMA GBC, Cu Kα radiation), field emission scanning electron microscopy (FESEM; JEOL-7500, 2 keV), and transmission electron microscopy (TEM; JEOL-2010, 200 keV). Thermogravimetric analysis was conducted on a TA 2000 Thermo-analyzer. The electrochemical tests were carried out *via* CR2032 coin type cells. The working electrodes were prepared by mixing the as-prepared Ge@C, Ketjenblack, sodium carboxymethyl cellulose, and polyacrylic acid at a weight ratio of 80 : 10 : 5 : 5. The resultant slurry was pasted on Cu foil and dried in a vacuum oven at 150 °C for 5 h. The weight of the active materials on individual electrodes is 1 ± 0.2 mg. Coin cells were assembled in an argon-filled glove box (Mbraun, Unilab, Germany) by stacking a porous polypropylene separator containing a liquid electrolyte between the composite electrode and a lithium foil counter electrode. The electrolyte consisted of a solution of 1 M $LiPF_6$ in ethylene carbonate/dimethyl carbonate/diethyl carbonate (EC/DMC/DEC; 3/4/3 v/v; Novolyte) with 5 wt% fluoroethylene carbonate (FEC) additive. Cyclic voltammograms were collected on a VMP-3 electrochemical workstation at a scan rate of 0.1 mV s^{-1}. The discharge and charge measurements were conducted on a Land CT2001A battery tester and the rate performance was measured on an Arbin tester. At least five parallel cells were tested for each electrochemical measurement, in order to make sure that the results are reliable and represent the typical behavior of the samples.

Results and discussion

The formation of the hollow GeO_2 precursor is illustrated in Fig. 1 and the corresponding field emission-scanning electron microscopy (FE-SEM) images of GeO_2 precursors at different reaction times are presented in Fig. S1 in the ESI.† In a basic solution, the hydrolysis of Ge^{4+} and Sn^{4+} can occur simultaneously to generate insoluble GeO_2 and $Sn(OH)_4$ white precipitates, as shown in Fig. S1(a) and (b).† In order to minimise the free energy, the small nanoparticles gradually self-assemble to form large ellipsoids. Simultaneously, gradual dissolution of the $Sn(OH)_4$ templates also takes place due to the basic etching under continuous ultrasonication. When the reaction time reaches 120 min, GeO_2 hollow ellipsoidal structures with well-defined interiors and compact shells are eventually formed after complete dissolution of the $Sn(OH)_4$. $Sn(OH)_4$ was selected as the template because it has good material compatibility with GeO_2 and can slowly dissolve in a basic solution under continuous ultrasonication, while the GeO_2 precipitate can only dissolve in strong basic or acidic solution; therefore, in principle, the hollow structure can be generated as a result of simultaneous etching of the $Sn(OH)_4$ template. The volume of the hollow interior can also be adjusted by the reaction time of the ultrasonication and the ratio of $GeCl_4$ to $SnCl_4$ in the starting materials. The crystallographic structures of samples with different reaction times were determined by X-ray diffraction as shown in Fig. S2.† Except for the reaction time of 5 min, the diffraction patterns of all of the other samples can be

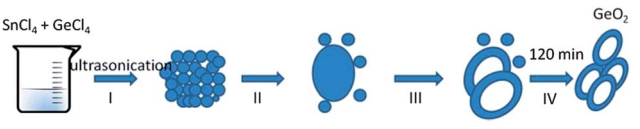

Fig. 1 Schematic illustration of the formation of GeO_2 hollow structures: (I) co-precipitation of GeO_2 and $Sn(OH)_4$ nanoparticles, (II) self-assembly of nanoparticles under ultrasonication, (III) continuous growth and dissolution of $Sn(OH)_4$ cores by basic etching, and (IV) formation of GeO_2 hollow ellipsoidal structures.

indexed to hexagonal GeO_2 (PDF # 36-1463), and no peaks indexed to $Sn(OH)_4$ can be observed due to its poor degree of crystallinity; therefore, in order to detect the Sn content in the samples, energy dispersive X-ray spectroscopy (EDS) analysis was employed to detect the elemental distribution. As shown in Fig. S3,† we can observe that the peaks of Sn gradually become weaker in intensity from 5 min reaction time to 90 min, and after 120 min, the peak ascribed to Sn was not observed, which further indicates that $Sn(OH)_4$ has dissolved completely after 120 min in the basic solution under ultrasonication.

In order to gain more insight into the effects of the ratio of $GeCl_4$ to $SnCl_4$ as starting materials on the hollow ellipsoid morphology, a series of ratio-dependent experiments ($Ge^{4+} : Sn^{4+} = 1 : 1$, $1 : 0.5$, and $1 : 0$ with the resultant samples denoted as GeO_2-1, GeO_2-2, and GeO_2-3, respectively) were conducted. The morphology and microstructure of these three samples were also characterized using FE-SEM and transmission electron microscopy (TEM), as shown in Fig. 2. A panoramic view from Fig. 2(a) and (d) reveals that in the presence of $SnCl_4$ as the starting material, a large amount of uniform GeO_2 ellipsoids with an average diameter of 300–400 nm was obtained after ultrasonication for 120 min. The FE-SEM images in Fig. 2(b) and (e) clearly display the hollow nature of the GeO_2 particles from the cracked ellipsoid, but with the ratio of $GeCl_4$ to $SnCl_4$ increased to $1 : 0.5$, the surfaces of the hollow ellipsoids become rougher, as shown in Fig. 2(e), compared to GeO_2-1 in Fig. 1(b). In the absence of $SnCl_4$ in the starting material, the size distribution of the ellipsoids is still uniform, as shown in Fig. 2(g), but the hollow structure is not observed and the centre of the ellipsoids is nearly solid, as shown in Fig. 2(h). The volume of the ellipsoids also becomes larger, with a diameter of 500–600 nm, and in addition, the surfaces of the individual ellipsoids are rougher compared to samples GeO_2-1 and GeO_2-2, which can be ascribed to the increased size of the particles assembled into the ellipsoids without the addition of $SnCl_4$. The TEM images in Fig. 2(c), (f) and (i) show notable contrast differences between the hollow and the solid parts, which further gives evidence that the hollow volume decreases with increasing ratio of $GeCl_4$ to $SnCl_4$, and the size of the ellipsoids becomes significantly larger without the addition of $SnCl_4$. This indicates that the morphology of the GeO_2 precursor can be adjusted easily by adjusting the $SnCl_4$ content.

It has been reported previously that carbon is a good matrix to accommodate the volume change for group IVA elements (Si, Ge, and Sn) during the charge–discharge processes in lithium ion batteries. In this work, in order to reduce the GeO_2 to germanium metal and retain the hollow structure after annealing, acetylene was selected to serve both as a reducing agent to partially transform the GeO_2 to germanium metal (Ge) and simultaneously as a carbon source to wrap the resultant Ge ellipsoid. The carbon film that is decomposed from acetylene can be formed uniformly on the surfaces of the hollow structures, and many void spaces between the germanium nanoparticles can be generated at the same time. This carbon shell

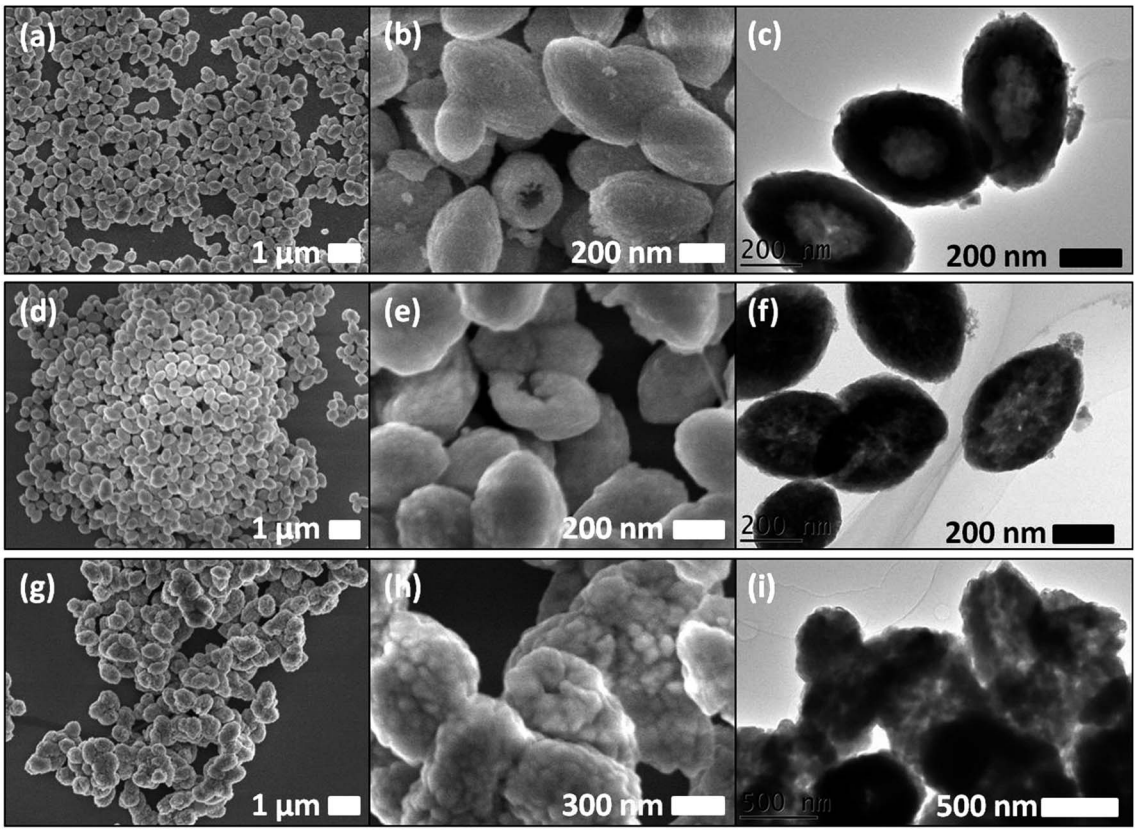

Fig. 2 Typical FE-SEM (a, b, d, e, g and h) and TEM (c, f and i) images for (a–c) GeO_2-1, (d–f) GeO_2-2, and (g–i) GeO_2-3.

can further enhance the electrical conductivity of all the active material, and more importantly, it can act as a matrix to accommodate the volume change during the alloying reaction and protect the integrity of the initial hollow structure, as well as preventing the continual formation of a solid electrolyte interphase (SEI) layer.[9] X-ray diffraction (XRD) was used to characterize the Ge@C ellipsoids (Ge@C-1, Ge@C-2, and Ge@C-3), as shown in Fig. S4.† The diffraction patterns of these three samples can be indexed to pure Ge with diamond cubic phase (PDF#04-0545, $a = 5.6576$ Å), and no impurity phase was detected in any of the three patterns, indicating that GeO_2 was fully reduced to pure Ge at 650 °C in the C_2H_2/Ar and H_2/Ar atmospheres. In addition, Raman spectroscopy was also performed on both the GeO_2 precursors and Ge@C for the two composite samples, as shown in Fig. S5.† The Raman spectra of GeO_2 in Fig. S5(a)† show peaks that match well with previous reports in the literature,[4] and all of the peaks can be related to the vibrations from GeO_2. The Raman spectra in Fig. S5(b)† confirm the presence of crystalline Ge, which is represented by a sharp peak at 292 cm^{-1}, and the two other peaks detected at 1317 and 1590 cm^{-1} can be ascribed to the D and G bands of carbon. The level of surface oxidation of Ge after reduction was investigated by Fourier transform infrared (FTIR) spectroscopy (Fig. S6†). Compared to the GeO_2 precursor, no typical GeO_2 peaks were detected in the Ge@C, which further indicates that GeO_2 was totally reduced to Ge, in agreement with the results from XRD. The carbon contents of the three samples were investigated by thermogravimetric analysis (TGA), as shown in Fig. S7.† They were determined to be 16.7%, 14%, and 5.8% in Ge@C-1, Ge@C-2, and Ge@C-3, respectively. To further understand the porous nature of the Ge@C (1–3) samples, N_2 adsorption–desorption isotherms were collected as shown in Fig. S8(a)–(c),† and all of these three samples show a typical IV isotherm shape, consistent with mesoporosity. The Brunauer–Emmett–Teller (BET) surface areas for the Ge@C (1–3) samples were determined to be 48, 41, and 31 $m^2\ g^{-1}$, respectively. The pore size distribution (the inset of Fig. S8†) indicates that the majority of pores in the Ge@C-1 sample are around 30 nm in diameter, and the pore size becomes smaller (~15 nm) for Ge@C-2, while the pore size for the Ge@C-3 sample is distributed randomly in the range from 10 to 50 nm, compared to other two samples. This indicates the mesoporous nature of the hollow Ge@C ellipsoids.

Further morphological and structural characterizations were carried out using both FE-SEM and high resolution TEM (HR-TEM) microscopic methods. Fig. S9(a)–(c)† present typical low-magnification FE-SEM images of the Ge@C (1–3) ellipsoids, which showed a similar morphology to their GeO_2 precursors. The magnified FE-SEM images, as shown in Fig. S9(d)–(f),† clearly indicate that the ellipsoidal structure can be retained after annealing in the acetylene atmosphere, and the cracked ellipsoid also demonstrates the hollow nature of the Ge@C-1 and Ge@C-2 ellipsoids. In addition, the TEM images in Fig. 3(a)–(c) show that after acetylene decomposition, a uniform carbon layer was deposited on the particle surfaces as a shell. For these three samples (Fig. 3(a)–(c)), many voids and pores appeared between the Ge nanoparticles due to the associated volume changes and gas release from the reduction of GeO_2 to Ge. The TEM images in Fig. 3(d)–(f) indicate that the Ge nanoparticles are wrapped intimately within carbon shells, and the thickness of the carbon shell is in the range of 3.6–9 nm for Ge@C-1 and ~7 nm for Ge@C-2 and Ge@C-3, respectively. The selected-area electron diffraction (SAED) pattern (the inset of Fig. 3(a)) also reveals the nature of the Ge, and these visible diffraction rings can be indexed to the diamond cubic Ge phase, which is consistent with the XRD patterns. The calculated *d*-spacings from the crystal lattice fringes for Ge@C-1, Ge@C-2, and Ge@C-3 in Fig. 3(d)–(f) are the same (0.32 nm), which can be assigned to the (111) plane of cubic Ge. Based on the TEM images, it could be further confirmed that the Ge nanoparticles are coated by a uniform carbon layer, and the pores and voids formed after reduction from GeO_2 to Ge can further provide more space to accommodate the volume expansion during alloying/de-alloying processes, which would enhance the

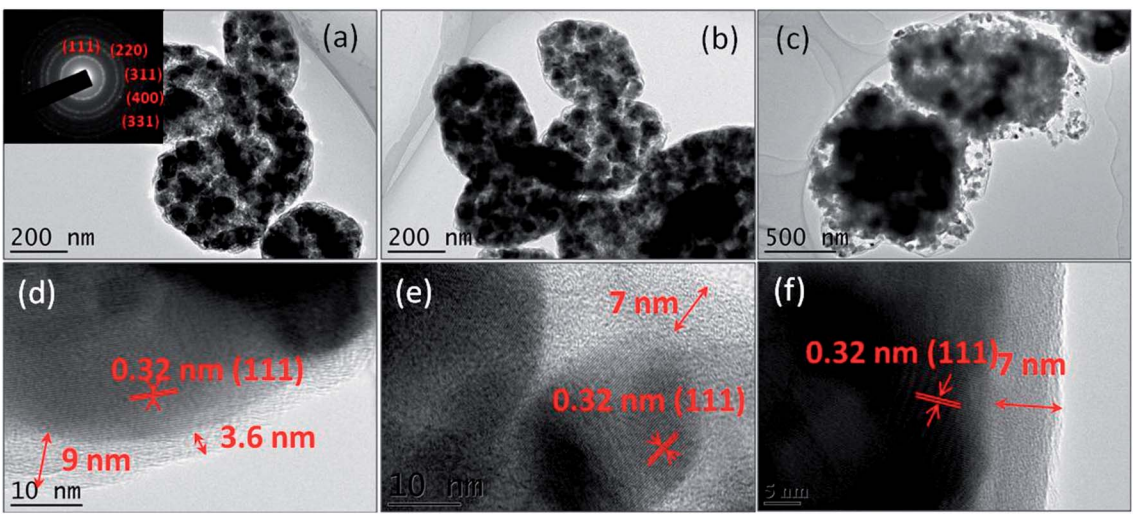

Fig. 3 TEM images at different resolutions of (a and d) Ge@C-1, where the inset of (a) is the corresponding SAED pattern of Ge; (b and e) Ge@C-2; (c and f) Ge@C-3.

cycling stability of Ge as an anode material for LIBs. For comparison, we also reduced the GeO_2 precursor directly through a flowing H_2/Ar atmosphere, without the flowing acetylene/Ar. As shown in Fig. S10,† it should be noted that the ellipsoidal structure was totally destroyed, and the particles are aggregated together.

The electrochemical performance of Ge@C-1 and Ge@C-3 was tested by the galvanostatic discharge–charge technique between 0.01 and 1.5 V in coin-type half-cells. Fig. 4(a) shows the first cycle voltage profiles of both samples, and the voltage profiles of both samples at the 2nd, 10th, and 50th cycle are shown in Fig. S11.† The first discharge and charge capacities for Ge@C-1 were 1554 and 1220 mA h g^{-1}, respectively, corresponding to the Coulombic efficiency of 78.5%. This is lower than that of Ge@C-3, for which the first discharge and charge capacities of 1680 and 1365 mA h g^{-1} were recorded, and the corresponding Coulombic efficiency was 81.25%. The reason for the lower Coulombic efficiency of Ge@C-1 can be ascribed to the smaller particle size and larger surface area, which results in more surface area for SEI formation. In order to understand the electrochemical reactions of the Ge@C electrode, cyclic voltammetry (CV) was performed at a scan rate of 0.1 mV s^{-1}. The CV curves for the first 5 cycles of Ge@C-1 are presented in Fig. S12.† During the 2nd reduction process, four peaks located at 0.5, 0.34, 0.17, and 0.08 V can be detected, respectively, which correspond to the lithium alloying reaction to form different Li–Ge phases. In the corresponding oxidation process, the peak at 0.6 V indicates the de-alloying reaction of Li_xGe. In the subsequent cycling, the peaks exhibit no shifts, indicating highly reversible lithiation/delithiation of Ge@C as an anode material for LIBs.

Fig. 4(b) shows the cycling performance of both samples, first at 0.1 C for 5 cycles, then at the 0.2 C rate (1 C = 1600 mA g^{-1}) for 200 cycles. It can be seen that although the capacity of Ge@C-3 was higher than that of Ge@C-1 for the first 50 cycles, the capacity of Ge@C-3 faded gradually for the subsequent cycles, and at the 200th cycle, the capacity retention recorded was 83% (1137 mA h g^{-1}). In contrast, no capacity fading was observed for Ge@C-1, and the capacity retention is nearly 100% (1285 mA h g^{-1}) after 200 cycles. In addition, although a large irreversible capacity loss was observed in the first cycle, the reversibility of the capacity was significantly improved afterwards, with an average Coulombic efficiency of 99% for up to 200 cycles. The reason for the lower capacity for Ge@C-1 in the initial 50 cycles at 0.2 C compared to Ge@C-3 can be ascribed to the larger surface area and higher carbon content for Ge@C-1, which would lead more SEI formation and reduce the capacity of the electrode. Furthermore, the cycling performance for both samples was also tested at the 1 C rate. The results were similar to the results at 0.2 C, with Ge@C-3 exhibiting a slightly higher capacity than Ge@C-1 for the first 70 cycles, but the difference in the capacity between these two samples decreased significantly after that. Additionally, the specific capacity for Ge@C-1 showed a slight fading up to 200 cycles, where a charge capacity of 1140 mA h g^{-1} was recorded, 90% of the capacity at the 5th cycle. The capacity retention for Ge@C-3 was 81.4% (1083 mA h g^{-1}) after 200 cycles. The capacity is still considerably higher, however, than in previous reports in the literature.[6,10] The high capacity and excellent cycling stability of the Ge@C-1 sample can be attributed to the hollow structure and porous carbon shells, which can accommodate the volume changes during lithium reactions. In addition, the porosity of the hollow carbon

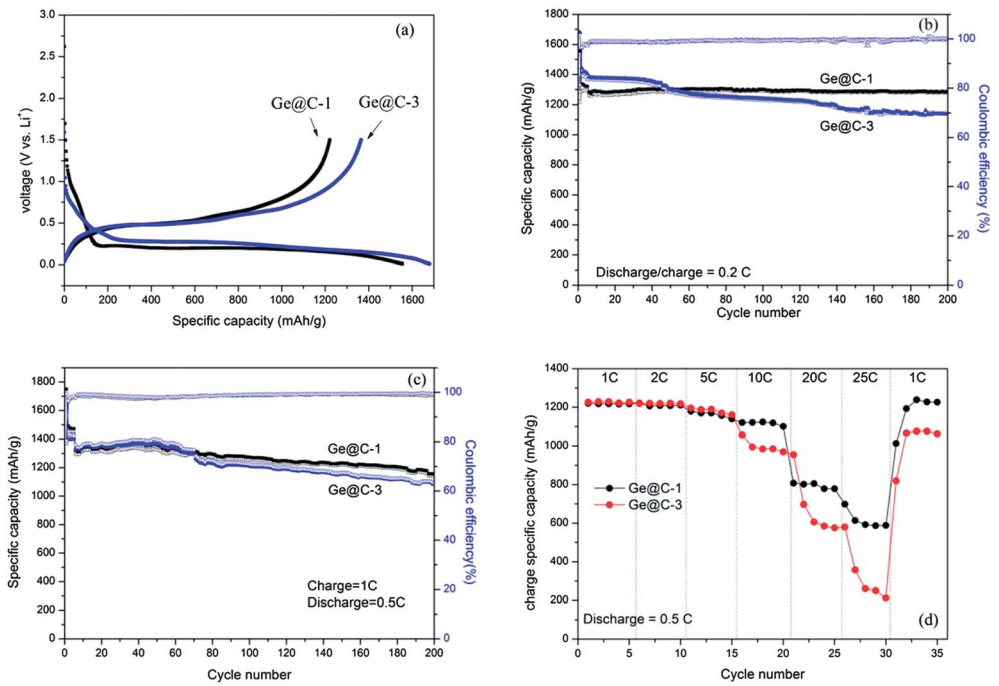

Fig. 4 (a) Voltage profiles of Ge@C samples at the first discharge–charge cycle at the 0.1 C/0.1 C rate in the voltage range of 0.01–1.5 V; (b and c) cycling performance of the Ge@C samples at the 0.2 C/0.2 C rate and the 1 C/0.5 C rates, respectively; (d) rate performance of the Ge@C samples with increasing rates from 1 to 25 C.

shells can also facilitate contact of the electrolyte with the germanium nanoparticles. In contrast, the solid structure and lower surface area of Ge@C-3 would lead to limited space to accommodate volume expansion during cycling, which results in poor cycling stability.

The rate capability of Ge@C-1 and Ge@C-3 for charging is shown in Fig. 4(d). For both samples, the discharge rate was fixed at the 0.5 C rate. At the lower rates (1 C, 2 C, and 5 C), the trend in the capacity change for both samples is very similar; there is marginal capacity fading as the rate increases. When the rate is increased from 10 C to 25 C, however, the Ge@C-3 sample presents poor capacity retention compared to Ge@C-1. The average charge capacity for Ge@C-3 was 984, 584, and 260 mA h g^{-1} at rates of 10 C, 20 C, and 25 C, respectively, and these values correspond to 80%, 48%, and 21% of the charge capacity at the 1 C rate, but the capacity could be nearly completely recovered when the rate was returned to 1 C. In contrast, Ge@C-1 exhibited good rate performance at high rates. There is a slight capacity decay observed up to 10 C, and the capacity retention value when the rate is increased to 20 C is 66% (805 mA h g^{-1}) of the capacity at 1 C, which is much higher than that in previously reported work on germanium.[10b,f,11] When the rate was further increased to 25 C, the capacity recorded was 592 mA h g^{-1}, which is still higher than the theoretical capacity of graphite (372 mA h g^{-1}). When the rate was returned to the 1 C rate, the capacity recorded was the same as that in the initial cycle at the 1 C rate. The corresponding voltage profiles at different rates for both samples are presented in Fig. S13(a) and (b).† With increasing C-rate, the polarization for Ge@C-3 is much higher than for the Ge@C-1 sample, in agreement with the results in Fig. 4(a). In addition, the cycling performance at 5 C was also tested for both samples, as shown in Fig. S12(c).† The trend in capacity decay is similar to the trend in cycling performance at the 1 C rate. The capacity of Ge@C-1 and Ge@C-3 was 977 and 628 mA h g^{-1} after 90 cycles, respectively, which corresponds to 79.6% and 51% of the capacity at 1 C. This further indicates that Ge@C-1 exhibits better cycling stability, particularly at high rate, and the reason can be ascribed to the high surface area and large pore size of the hollow structures, which can accommodate volume expansion during charging–discharging processes. In addition, the carbon content in Ge@C-1 and Ge@C-3 is different, which may affect the electrochemical performance, so in order to exclude this issue, we synthesized an additional sample, Ge@C-4, at 750 °C, with the other conditions kept the same as for Ge@C-3. The carbon content of Ge@C-4 is 21.6%, which is very close to that of Ge@C-1. The rate performance of Ge@C-4 is shown in Fig. S14.†

Conclusion

In summary, we have designed mesoporous and hollow germanium@carbon nanostructures (Ge@carbon) through simultaneous carbon coating and reduction of a hollow ellipsoidal GeO_2 precursor. The precursor was prepared through a facile one-pot ultrasonication method. Furthermore, we investigated the formation mechanism of the GeO_2 ellipsoids and found that controlling the ratio of Ge^{4+} to Sn^{4+} generates different hollow volumes. The hollow ellipsoidal Ge@C-1 sample exhibits better cycling stability (100% capacity retention after 200 cycles at the 0.2 C rate) and higher rate capability (805 mA h g^{-1} at 20 C) than the solid ellipsoidal sample (Ge@C-3). The excellent electrochemical performance can be ascribed to the unique hollow structure, which provides more voids and pores for accommodation of volume expansion, as well as the uniform carbon film on the surfaces of the Ge nanoparticles, which maintains their structural integrity and enhances the electronic conductivity of the whole electrode; therefore, this hollow ellipsoidal Ge@carbon structure can be considered as a potential anode material for lithium ion batteries.

Acknowledgements

This work was funded by an Australian Research Council (ARC) Discovery Project (DP1094261). The authors also would like to thank Dr Tania Silver at the University of Wollongong for critical reading of the manuscript. The authors acknowledge the use of facilities within the UOW Electron Microscopy Centre.

Notes and references

1 (*a*) M. S. Whittingham, *MRS Bull.*, 2008, **33**, 411; (*b*) M. Armand and J. M. Tarascon, *Nature*, 2008, **451**, 652.
2 (*a*) Y.-K. Sun, S.-T. Myung, B.-C. Park, J. Prakash, I. Belharouak and K. Amine, *Nat. Mater.*, 2009, **8**, 320; (*b*) T. Ogasawara, A. Débart, M. Holzapfel, P. Novák and P. G. Bruce, *J. Am. Chem. Soc.*, 2006, **128**, 1390; (*c*) X. L. Ji, K. T. Lee and L. F. Nazar, *Nat. Mater.*, 2009, **8**, 500.
3 (*a*) C. S. Fuller and J. C. Severiens, *Phys. Rev.*, 1954, **96**, 21; (*b*) J. Graetz, C. C. Ahn, R. Yazami and B. Fultz, *J. Electrochem. Soc.*, 2004, **151**, A698; (*c*) D. Wang, Y.-L. Chang, Q. Wang, J. Cao, D. B. Farmer, R. G. Gordon and H. Dai, *J. Am. Chem. Soc.*, 2004, **126**, 11602.
4 (*a*) K. H. Seng, M.-H. Park, Z. P. Guo, H. K. Liu and J. Cho, *Angew. Chem., Int. Ed.*, 2012, **51**, 5657; (*b*) K. H. Seng, M. H. Park, Z. P. Guo, H. K. Liu and J. Cho, *Nano Lett.*, 2013, **13**, 1230.
5 H. Lee and J. Cho, *Nano Lett.*, 2007, **7**, 2638.
6 (*a*) M.-H. Park, Y. Cho, K. Kim, J. Kim, M. Liu and J. Cho, *Angew. Chem., Int. Ed.*, 2011, **50**, 9647; (*b*) C. K. Chan, X. F. Zhang and Y. Cui, *Nano Lett.*, 2007, **8**, 307.
7 Y. Xiao, M. Cao, L. Ren and C. Hu, *Nanoscale*, 2012, **4**, 7469.
8 (*a*) J. Hu, M. Chen, X. Fang and L. Wu, *Chem. Soc. Rev.*, 2011, **40**, 5472; (*b*) X. Lai, J. E. Halpert and D. Wang, *Energy Environ. Sci.*, 2012, **5**, 5604; (*c*) X. W. Lou, L. A. Archer and Z. Yang, *Adv. Mater.*, 2008, **20**, 3987; (*d*) Q. Zhang, W. Wang, J. Goebl and Y. Yin, *Nano Today*, 2009, **4**, 494.
9 N. Liu, H. Wu, M. T. McDowell, Y. Yao, C. Wang and Y. Cui, *Nano Lett.*, 2012, **12**, 3315.
10 (*a*) G. Cui, L. Gu, N. Kaskhedikar, P. A. van Aken and J. Maier, *Electrochim. Acta*, 2010, **55**, 985; (*b*) G. Cui, L. Gu, L. Zhi, N. Kaskhedikar, P. A. van Aken, K. Müllen and J. Maier, *Adv. Mater.*, 2008, **20**, 3079; (*c*) R. A. DiLeo, S. Frisco, M. J. Ganter, R. E. Rogers, R. P. Raffaelle and B. J. Landi,

J. Phys. Chem. C, 2011, **115**, 22609; (*d*) M. G. Kim and J. Cho, *J. Electrochem. Soc.*, 2009, **156**, A277; (*e*) Y.-D. Ko, J.-G. Kang, G.-H. Lee, J.-G. Park, K.-S. Park, Y.-H. Jin and D.-W. Kim, *Nanoscale*, 2011, **3**, 3371; (*f*) M.-H. Seo, M. Park, K. T. Lee, K. Kim, J. Kim and J. Cho, *Energy Environ. Sci.*, 2011, **4**, 425; (*g*) L. C. Yang, Q. S. Gao, L. Li, Y. Tang and Y. P. Wu, *Electrochem. Commun.*, 2010, **12**, 418; (*h*) Z. Yang and J. G. C. Veinot, *J. Mater. Chem.*, 2011, **21**, 16505; (*i*) S. Yoon, C.-M. Park and H.-J. Sohn, *Electrochem. Solid-State Lett.*, 2008, **11**, A42.

11 D.-J. Xue, S. Xin, Y. Yan, K.-C. Jiang, Y.-X. Yin, Y.-G. Guo and L.-J. Wan, *J. Am. Chem. Soc.*, 2012, **134**, 2512.

